Environmental Fluid Mechanics (2005) 5: 267–292
DOI 10.1007/s10652-004-3820-2

Double-Arranged Mound-Mounted Shelterbelts: Influence of Porosity on Wind Reduction between the Shelters

C. FRANK* and B. RUCK
Laboratory of Building- and Environmental Aerodynamics, Institute for Hydromechanics, University of Karlsruhe, Kaiserstrasse 12, 76128 Karlsruhe, Germany

Received 26 January 2004; accepted in revised form 26 September 2004

Abstract. Using a two-dimensional LDA-System, measurements in an atmospheric boundary layer wind tunnel have been made in the intermediate field of double-arranged, mound-mounted shelterbelts. The porosity of the shelterbelts ranged from 0% to 52%. For each porosity, seven different distances of the two windbreaks between 5 and 25 times the windbreak height were investigated. The efficiency of the windbreak systems is assessed by means of protection parameters considering the change of horizontal momentum on bodies immersed in the flow, of pedestrian comfort conditions and of momentum exchange in vertical direction. Furthermore recirculation zones and the change of kinetic energy are shown. The measurement results are given in the form of contour plots indicating flow quantities and protection volumes between the two windbreaks. The shelter efficiency of the investigated windbreak systems is compared to that of adequate single line windbreaks. It is shown that for certain windbreak configurations the wind-protected area in the intermediate field of consecutively arranged windbreaks becomes larger in comparison to a single windbreak.

Key words: atmospheric boundary layer, mound, porosity, protection volume, shelterbelt, windbreak, wind tunnel experiments

1. Introduction

Due to a rising environmental awareness and augmented requirements in emission control, windbreaks play an important role, particularly in the urban and industrial domain. In order to protect areas against wind attacks, not only single lines of windbreaks are erected at the windward side, but also windbreak systems surrounding whole areas or industrial sites. Thus, in many cases the area between can be conceived of as being protected by a windward and a leeward windbreak (double-arrangement). Since the horizontal extent of the wind shelter efficiency is usually assumed to be proportional to windbreak height, shelterbelts are often mounted on thrown-up earth walls (mounds) in order to obtain an increased shelter.

*Corresponding author, E-mail: frank@ifh.uni-karlsruhe.de

Preferentially, double-arranged windbreaks are erected e.g., around dumpsites, transhipment areas or industrial sites where bulk material is likely to be dispersed by the atmospheric flow. Thus, the wind activity over industrial sites can be calmed-down by an adequate windbreak arrangement yielding a maximum reduction of advective flow quantities in the protected zone between. An optimised layout of the wind shelter efficiency of such double-arranged windbreak systems allows an efficient reduction of immissions in adjacent densely populated areas.

Windbreaks and shelterbelts are the subject of active research for many decades, however, the search for an optimum arrangement is difficult with varying boundary conditions. Despite of numerous investigations, a full understanding of the aerodynamics of windbreaks is still not available, especially for windbreaks on mounds. A survey of early investigations is given by Van Eimern [1] and several more up-to-date reviews followed [e.g., 2–4].

The fluid mechanical principle of the most frequently investigated windbreak arrangement – linear porous belt resting on a uniform surface – is well understood due to many experimental studies, both in nature [e.g., 5–8] and in wind tunnels [e.g., 9–14]. Most of them treat the wind reduction only near the ground and not in the space above. Besides physical models, numerical models were developed and applied in the last few decades in order to study the airflow through and around shelterbelts. Wang and Takle [15] used a numerical model to study the characteristics and patterns of flow and turbulence for a whole range of porous single line shelterbelts. Wang *et al*. reviewed in [16] recent results of their numerical simulations as well as the mechanisms controlling flow and turbulence around shelterbelts.

Despite of the practical relevance of multiple barrier systems, studies of arrays of windbreaks are rather rare. The results gained with single windbreaks are not simply applicable to multiple barriers. Judd *et al*. [17] concluded from their wind tunnel study that upstream members of an array of windbreaks act as an additional upstream roughness resulting in both, an overall decrease in wind speed and an increase in ambient turbulence. The consequence of the enhanced turbulence is that the effectiveness of a single windbreak within an multiple array is reduced compared to the shelter effect of an equivalent isolated windbreak. In a field study, McAneney and Judd [18] measured mean wind and turbulence within and above 15 parallel windbreaks and point out the difficulty of reducing simultaneously mean wind speeds and turbulence levels with a multiple windbreak system. Wilson and Yee [19] investigated the performance of different RANS wind models for multiple windbreak arrangements with the data of McAneney and Judd [18]. In contrary to simulations of single windbreaks, the predictions of all applied turbulence closure schemes seem to be not very accurate in the case of a multiple arrangement, even with respect to the mean

flow. They concluded that in very disturbed micro-meteorological flows, the present RANS wind models should not used yet as a stand-alone alternative to measurements.

The knowledge about the wind shelter efficiency of mound-mounted shelterbelts is limited to single line windbreaks [20, 21]. There is a lack of knowledge regarding double-arranged systems. It is assumed that depending on the structure and the distance between the windbreaks, counterproductive vortex formation may occur increasing the emissions from the site instead of reducing them.

The purpose of this paper is to present the results of a systematic study in an atmospheric boundary layer wind tunnel on double-arranged mound-mounted shelterbelts. Fundamental findings and relations between the relevant windbreak structural parameters are given in order to define optimum shelter efficiency for the field between the windbreaks. Besides other factors of influence, such as angle of mound, ratio of mound-height to shelterbelt-height and distance between the windbreaks, emphasis is laid in this paper on the influence of shelterbelt porosity. On the basis of two-dimensional LDA-measurements, the flow characteristics in the intermediate field are investigated yielding differently defined wind protection parameters. The shelter efficiency of the investigated double-arranged windbreak systems is compared to the efficiency of single line windbreaks [20, 21].

2. Experimental Methods

The experimental investigations have been carried out in the closed 29 m long boundary layer wind tunnel of the Laboratory of Building- and Environmental Aerodynamics at the Institute for Hydromechanics/University of Karlsruhe. A sketch of the wind tunnel test section and the velocity measurement system is shown in Figure 1. The test section has an 1.5 m octagonal cross-section and a length of 8 m. Using flow profile forming 'spires', triangular vortex generators and roughness elements, a natural atmospheric boundary layer could be simulated in the wind tunnel. The characteristics of the undisturbed approach flow are described below. The flow was allowed to develop over a fetch of 4 m and the atmospheric boundary layer reached at this point a depth of around 550 mm. The free stream velocity in the wind tunnel was checked by an anemometer and amounted to 5.55 m/s in a height of $z = 40$ cm for all investigations.

2.1. WINDBREAK MODELS

The windbreak models are sketched in Figure 2. The mounds below the actual shelterbelt models were made of wood; the porous thin shelterbelts

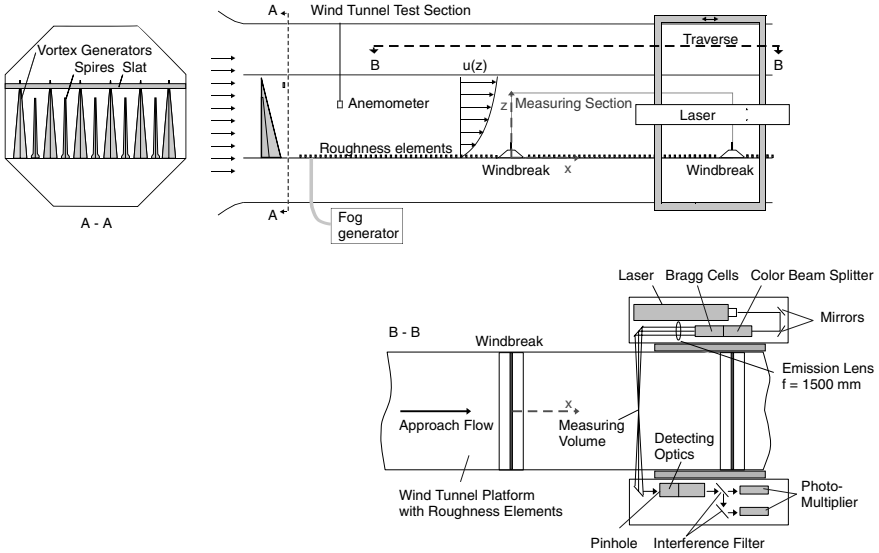

Figure 1. Sketch of the wind tunnel test section and the 2D-LDA-System.

were simulated from perforated sheets of Plexiglas. The overall height of the model windbreaks $(h + H)$ amounted to 12 cm. The porosity was realised by fine holes homogeneously distributed over the shelterbelt area. The fineness of the holes is defined by the ratio of hole-diameter D to thickness of the shelterbelt $B : D/B = 1$. The porosity is defined as the ratio of perforated area to total area. For thin artificial barriers $(H \gg B)$, as they were used here, the porosity can be assumed to be equal to the optical porosity deduced from the optically projected area of the shelterbelt.

The approach flow was set perpendicular to the windbreaks, whose length L (perpendicular to the flow direction) extended to 12.5 times the windbreak height ending in the lateral boundary layers of the wind tunnel sidewalls. Thus, it is assumed that the suppressed three-dimensional lateral

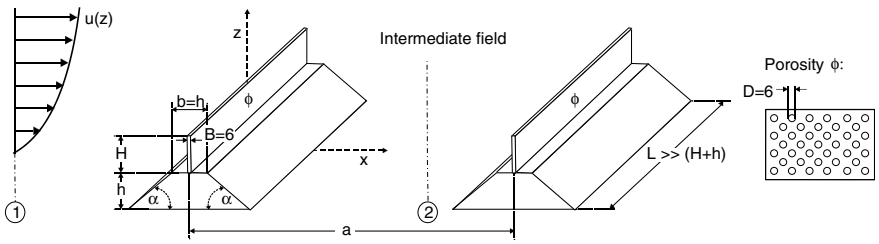

Figure 2. Sketch of the models and nomenclature used.

flow around the windbreak ends affects only slightly the results taken in the middle of the wind tunnel and that the two-dimensional case of two long parallel windbreaks is considered.

The origin of the used x, z-Cartesian co-ordinate system was located on the wind tunnel floor at the middle of the first (upstream) windbreak with the x-axis in horizontal streamwise direction and the z-axis in upward oriented vertical direction (Figures 1 and 2). The instantaneous velocity components are decomposed into temporal means and fluctuations: $U = u + u'$ in streamwise direction and $W = w + w'$ in vertical direction. In the following, the field between the two windbreaks is referred to as the intermediate field (Figure 2).

During the investigations, the ratio of mound-height to shelterbelt-height $h/H = 1$ and the angle of mound $\alpha = 40^\circ$ were kept constant. Seven different distances a between the two windbreaks were investigated in a range of $a/(h+H)$ between 5 and 25 for five different porosities ϕ, starting from 0% (impermeable shelterbelt) up to 52%.

2.2. VELOCITY MEASUREMENTS

The velocity measurements were accomplished by means of a two-component laser Doppler anemometer system (LDA) including an argon-ion laser (4 W) and two double bragg cells for frequency shifting (Figure 1). The LDA-signals were detected by photomultipliers in forward light scattering and were band-pass filtered in a range between 300 kHz and 1 MHz. The data were evaluated by counter-based electronics (2 TSI signal processors, Model IFA 550). The seeding was generated with an evaporation/condensation-type fog generator using 1,2-Propandiol as generator fluid (droplet diameter 1–2 μm).

The flow fields were measured between the two shelterbelts ($0 \le x \le a$) within a height from $z = 0.08 \cdot (h + H)$ to $z = 4.16 \cdot (h + H)$. Depending on the windbreak distance, between 5 and 13 different vertical profiles were sampled. Each vertical profile between the two windbreaks consists of 24 measuring points and the two profiles above the shelterbelts (first and last profile, $1.04 \cdot (h + H) \le z \le 4.16 \cdot (h + H)$) consist each of 16 measuring points. Near the ground, the measuring points lay closer together than in greater height. The measured values were interpolated linearly in vertical direction and according to the method of Aitken-Neville in horizontal direction in order to obtain uniform grids. Isoplots were then generated by means of these grids using the software SURFER 7.0. This software enables also to determine the size of areas with particular minimum or maximum values, that is the size of protection volumes.

2.3. SIMULATION OF THE ATMOSPHERIC BOUNDARY LAYER FLOW

In order to simulate real atmospheric flows in wind tunnels, the properties of the modelled flow have to be similar to those of the natural wind. Neutrally stratified atmospheric boundary layers can be characterized sufficiently by the profiles of the mean wind velocities and of the turbulence intensities as well as by the energy distribution of the gusts.

The vertical distribution of the mean horizontal velocity $u(z)$ in the test-section, normalized by the reference velocity $u_{\mathrm{ref}} = 3.2\,\mathrm{m/s}$ in a height $z_{\mathrm{ref}} = 0.05\,\mathrm{m}$, can be fitted well with the power law

$$\frac{u(z)}{u_{\mathrm{ref}}} = \left(\frac{z}{z_{\mathrm{ref}}}\right)^{\alpha}, \tag{1}$$

using a profile exponent $\alpha = 0.26$ (Figure 3a). Using a model scale 1:200, z_{ref} amounts to 10 m in nature. This height is often used in environmental aerodynamics as reference height. The profile exponent is typical for suburban terrain and forested areas, respectively, see [22, 23]. The velocity profile satisfied alternatively the logarithmic law-of-the-wall (Figure 3b)

$$u(z) = \frac{u_*}{k} \cdot \ln\left(\frac{z-d}{z_0}\right), \tag{2}$$

where k is the von Kármán constant and has a value of 0.4. The zero displacement d and the roughness length z_0 are 0 mm and 1.55 mm, respectively. z_0 amounts to 0.31 m in nature and corresponds, according to [24], to velocity profiles over suburban and industrial areas. The friction velocity u_* amounts to 0.367 m/s and thus the wall shear stress $\tau_0 = u_*^2 \cdot \rho$ is $0.165\,\mathrm{N/m^2}$. The logarithmic law-of-the-wall is only valid in the surface layer SL, where $y^* = u_* \cdot y/\nu$ ranged from 60–250 (bottom of SL) up to 5000–10000 (top of SL), see [25]. y^* of our measurements varies between

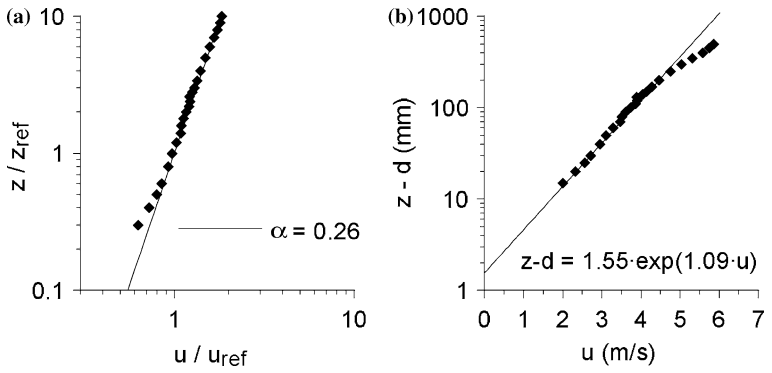

Figure 3. Simulated atmospheric boundary layer: mean longitudinal velocity (a) Power Law, (b) Law-of-the-wall.

280 ($z = 1$ cm) and 14100 ($z = 50$ cm). In a height of $z = 30$ cm ($z/z_{ref} = 6$), y^* amounts to 8500 and thus, this height can be considered as the top of the simulated SL. The Reynolds number of the boundary layer based on the reference point (with $u = 3.2$ m/s at $z = 0.05$ m) is about 12600.

The correlations of the velocity fluctuations exhibit a nearly constant behaviour in the lower part of the boundary layer (Figure 4a). This is typical for the surface layer (also referred to as constant flux layer) where the fluxes vary with height by less than 10% of their magnitude and where $u_*^2 = -u'w'$ applies [26]. The theoretical curve in Figure 4a is derived alternatively from the function of the vertical distribution of shear stress described in [27]

$$\tau(z) = -\tau_0 \cdot \left(1 - \frac{z}{\delta}\right)^{2\cdot\alpha+1}, \tag{3}$$

where the boundary layer height δ was assumed to be 350 m in nature.

The profiles of the turbulence intensities in mainstream direction T_u (Figure 4b)

$$T_u = \frac{\sqrt{u'^2}}{u} \tag{4}$$

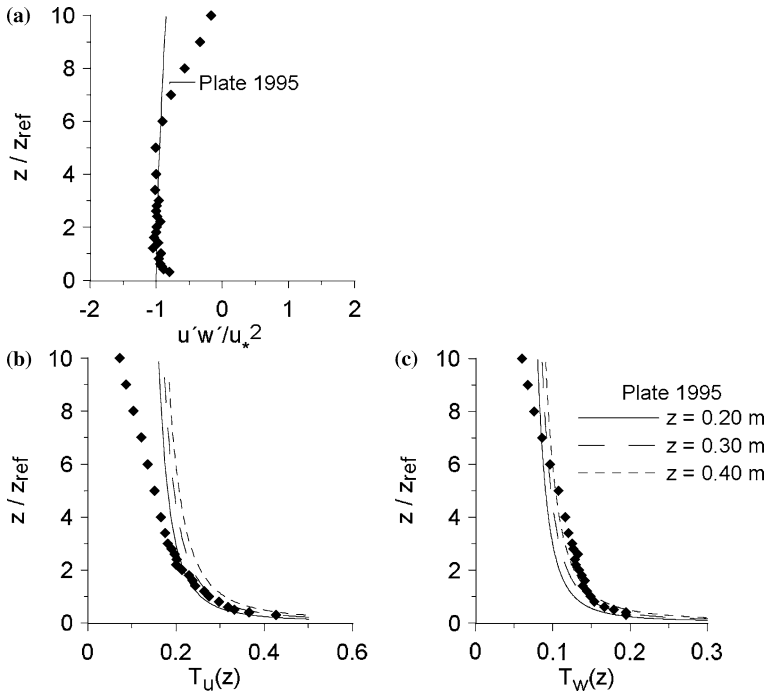

Figure 4. Simulated atmospheric boundary layer: (a) reynolds stress, (b) turbulence intensity in longitudinal direction, (c) turbulence intensity in vertical direction.

and in vertical direction T_w (Figure 4c)

$$T_w = \frac{\sqrt{w'^2}}{u} \tag{5}$$

are displayed over height. T_u amounts to 0.43 and T_w to 0.19 near the ground ($z/z_{\text{ref}} = 0.3$). Both quantities decrease gradually as the height z increases and agree reasonably with the theoretical distributions described in [23]

$$T_u(z) = 1/\ln((z-d)/z_0), \tag{6}$$

$$T_w(z) = 0.5/\ln((z-d)/z_0). \tag{7}$$

The integral length scale L_{ux} describes the size of the uniformly moved mass and thus the mean size of the eddies. It depends on both the type of terrain and the height above ground and is calculated by means of the correlation of the mainstream velocity component (cross-correlation in variable distances). According to Taylor's hypothesis of the 'frozen turbulence', this cross-correlation can be approximated by an autocorrelation of the detected velocity signal $R_{\text{uu}}(\tau)$

$$R_{\text{uu}}(\tau) = \lim_{T\to\infty} \frac{1}{T} \cdot \int_0^T u'(t) \cdot u'(t+\tau)dt, \tag{8}$$

where τ is the time lag. Taylor's hypothesis is applicable for $T_u(z) < 0.5$, see Stull [26]. The integral length scale is defined as

$$L_{\text{ux}} = u \cdot \frac{\int_0^\infty R_{\text{uu}}(\tau)d\tau}{\int_0^\infty R_{\text{uu}}(0)d\tau} = u \cdot \frac{\int_0^\infty R_{\text{uu}}(\tau)d\tau}{\sigma_u^2}, \tag{9}$$

where σ_u is the standard deviation of the horizontal velocity.

Unfortunately, the values of the natural atmospheric integral length scales found in the literature show a large scattering and complicate the comparison with the natural data. The Eurocode [24] suggests the following function:

$$\begin{aligned} &L_i(z) = 300 \cdot \left(\tfrac{z}{300}\right)^{\varepsilon} && \text{for } z_{\min} \le z \le 300 \text{ m}, \\ &L_i(z) = 300 \cdot \left(\tfrac{z_{\min}}{300}\right)^{\varepsilon} && \text{for } z \le z_{\min}, \\ &L_i(z) = 300 \text{ m} && \text{for } z > 300 \text{ m}, \end{aligned} \tag{10}$$

where (L_i, z in m) and $\varepsilon = 0.37$ for suburbs, industrial sites and forests. The comparison of the vertical distribution of the integral length scales in the wind tunnel with that of the Eurocode [24] shows, that the length scales

agree approximately (with a tendency to be smaller) in the lower part, but diverge in the upper part of the test section (Figure 5). The latter is not surprising, since the influence of the wind tunnel ceiling avoids a further increase of the integral length scale as in the natural, above-unbounded atmosphere.

Figure 6 shows the spectral density functions (Fourier transform of the autocorrelation function) of the modelled approach flow in two different heights, $z = 50$ mm and 200 mm. These are the result of the spectral analysis of the velocity time series in mainstream direction (x-direction). An often-applied function describing the spectral energy density $S_{uu}(f)$ in the atmospheric boundary layer is the von Kármán spectrum, which can be written

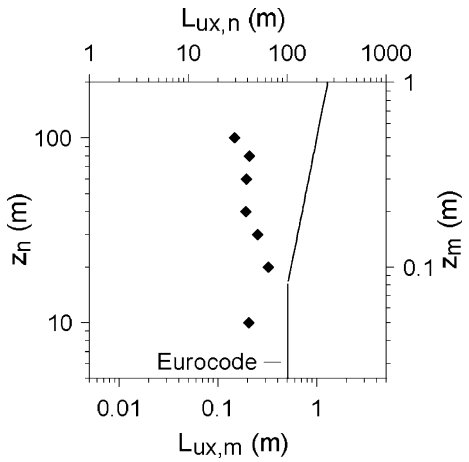

Figure 5. Simulated atmospheric boundary layer: integral length scale.

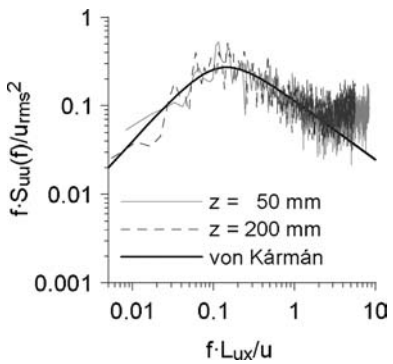

Figure 6. Simulated atmospheric boundary layer: spectral density function of the longitudinal velocity component.

as

$$\frac{f \cdot S_{\mathrm{uu}}(z, f)}{\sigma_u^2} = \frac{4 \cdot f_n}{[1 + 70.8 \cdot f_n^2]^{5/6}}. \tag{11}$$

Thereby the dimensionless frequency f_n was calculated with the integral length scale

$$f_n = \frac{f \cdot L_{\mathrm{ux}}}{u}. \tag{12}$$

A comparison of the dimensionless spectra in the wind tunnel boundary layer with that of the natural boundary layer (von Kármán spectrum) shows, that the spectral density functions agree very well with respect to the position and the value of their maximum. The decay of the spectra is proportional to $f^{-2/3}$ in the higher frequency range. Due to the finite frequency resolution of each measuring device and partly due to the loss of high frequencies as a result of scale reduction, the measured spectra in the wind tunnel exceed the theoretical values in the high frequency range.

3. Results and Discussion

The assessment of the effectiveness of windbreak systems can be performed with the aid of different protection parameters depending on measured flow quantities. In the following, the wind shelter effect of the investigated mound-mounted shelterbelts was assessed by protection parameters regarding the change of horizontal momentum on bodies immersed in the flow (Section 3.1), of pedestrian comfort (Section 3.2) and of vertical momentum exchange (Section 3.3). For each of these parameters adequate protection volumes were calculated. A protection volume was defined as an area in the intermediate field of two windbreaks, in which the particular protection parameter amounts to at least a pre-defined value, multiplied by the length L of a windbreak (perpendicular to the approach flow direction). The concept of protection volumes was introduced by Ruck and Donat [20,21]. Within the scope of this research work, sheltered volumes between double-arranged mound-mounted windbreak systems were determined for the first time as a function of porosity and windbreak distance. Moreover, observed recirculation zones (Section 3.4) and the change of kinetic energy (Section 3.5) are described.

In advance, it should be pointed out that not only the degree of perforation (the actual porosity) but also the hole size and the hole distribution are parameters influencing more or less the flow around the shelterbelt model. In this study, both parameters were kept constant. For more information on these aspects see e.g., Heisler and Dewalle [2], Gandemer [9], Wilson [28].

3.1. PROTECTION PARAMETER S_u

The protection parameter S_u

$$S_u(x, z) = 1 - \frac{u_2(x, z)^2}{u_1(z)^2} \tag{13}$$

is suitable to assess the reduction of the wind velocities and of the aerodynamic wind forces on bodies in the intermediate field of two windbreaks. This parameter refers at reference height z the local horizontal momentum fluxes of the disturbed (sheltered) flow field (Pos. 2 in Figure 2) to the momentum fluxes of the undisturbed (unsheltered) flow field in the approach flow (Pos. 1 in Figure 2). Since the aerodynamic force exerted on bodies is proportional to u^2, the protection parameter S_u indicates also the percentage of wind force reduction. If $S_u > 0$, the impact of wind forces decreases; if $S_u < 0$, it increases. The wind turbulence (gustiness) is not considered explicitly with this protection parameter.

Contour lines of three different protection parameters $S_u = 0.25$, 0.5 and 0.75 are shown in Figure 7 for varying porosities ϕ of the shelterbelt. In Figure 8 the dimensionless protection volume $v'_{Su} = V_{Su}/((h + H)^2 \cdot L)$ is shown over S_u for shelterbelts with porosities $\phi = 0\%$ and $\phi = 52\%$. A protection volume V_{Su} characterizes a zone in which the protection parameter amounts to at least S_u; zones with higher protection parameters are contained in it.

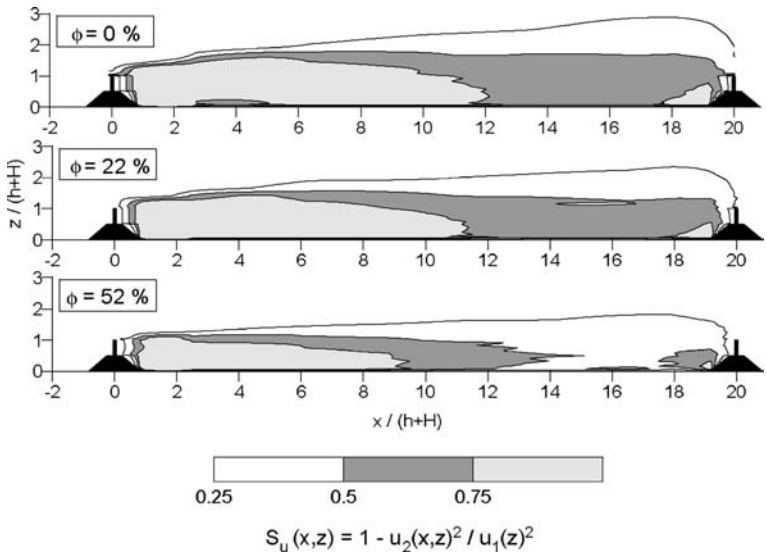

Figure 7. Contour lines of the protection parameter S_u as a function of porosity ϕ at a distance between windbreaks $a' = 20$.

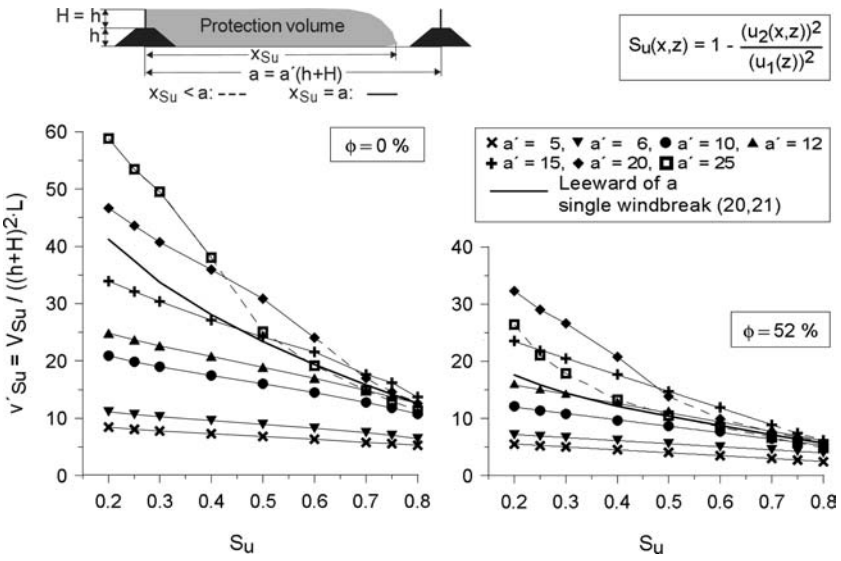

Figure 8. Dimensionless protection volume v'_{Su} as a function of protection parameter S_u with varying distance between windbreaks a' for two different porosities ϕ.

Figures 7 and 8 show that the porosity affects strongly the shelter efficiency of windbreak systems and thus the size of their protection volumes. With decreasing porosity, the size of the protected volumes increases. To realize the same single line protection volume with a double arrangement, the minimum distance between the lines is increasing with decreasing porosity (Figure 8). That is obvious, since the investigations of mound-mounted single windbreaks, accomplished by Ruck and Donat [20, 21], reveal that with decreasing porosity not only the size of the protection volume V_{Su} but also its length x_{Su} increases (see Table I). This can also be seen in Figure 7 for $S_u = 0.75$.

Provided that the intermediate field is protected over its whole length ($x_{Su} \cong a$), protection volumes between two windbreaks possess a more uniform shape than protection volumes leeward of an adequate single windbreak having the same size.

Furthermore, it can be observed that the influence of the leeward arranged second windbreak diminishes with rising reduction of the aerodynamic wind force. In comparison to single windbreaks, areas with low shelter effect (low S_u values) can be enlarged much more by a double arrangement with well-chosen distance than areas with high shelter effect (high S_u values). In other words, a double arrangement of windbreaks is effective when compared to a single windbreak mainly for low to medium required wind shelter.

Table I. Dependence of observed maximum extent of wind velocity reduction leeward of single line windbreaks and leeward of the upstream windbreaks of double-arrangements upon porosity. The values give the downwind distance in multiples of shelterbelt height at which the reduced velocity recovers to 50% (70%) of the upstream wind velocity.

Porosity (%)	Single windbreaks				Double-arrangement
	without mound			with mound	($H/h=1,\ \alpha=40°$)
	Raine and Stevenson [12]	Wang and Takle [15]	Lieff [14]	Ruck and Donat [20]	Our investigation ($a'=25$)
0	11.8 (16)		13.5	12.1 (15.8)	11.1 (16.0)
8		6.5 (8.7)			
12			14.6	12.1 (15.6)	10.6 (15.0)
20/22	*12 (16.2)*		14.2	11.7 (14.9)	10.6 (14.8)
30			13		
34/35	*9.8 (14)*			11.0 (13.8)	10.3 (13.6)
40		11.7 (15.5)			
50/52	*7.8 (11.9)*		*12.5*	9.4 (12.1)	9.6 (12.0)
H/z_0	100	200	470	133	77.4

Figure 9 shows the dimensionless protection volume $v'_{Su} = V_{Su}/((h + H)^2 \cdot L)$ over the reduction of the aerodynamic wind force (the protection parameter S_u) for double-arranged windbreaks with varying windbreak distances a'.

The influence of porosity increases with increasing windbreak distance. This means that, at small distances (Figure 9a), the protection volumes between medium dense windbreaks are a little smaller than those between impermeable windbreaks. With increasing distance, however, the difference in protection volume size increases (Figures 9b, 9c). This applies at least so long as the protection volumes between the denser windbreaks extend across the entire length of the intermediate field ($(x_{Su} \cong a)$, solid lines in Figure 9).

As far as the windbreak distance becomes larger than the length of the maximal protected area (area with $S_u = 0.8$), a linear dependence between the protection volume V_{Su} and the protection parameter S_u exists for the respective distance. Thereby the porosity-dependent curves run approximately parallel to each other. In agreement to the single windbreak it applies also here that denser windbreaks cause larger protection volumes. That was observed at every investigated distance.

The differences in size of protection volumes with varying minimum shelter effect (varying parameters S_u) increase likewise with increasing

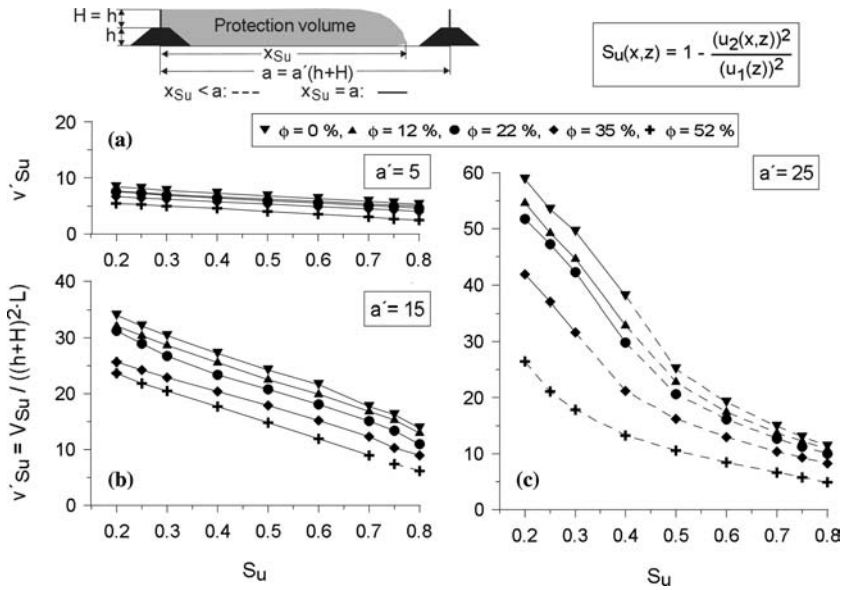

Figure 9. Dimensionless protection volume v'_{Su} as a function of the protection parameter S_u with varying porosity ϕ for different distances between windbreaks a'.

windbreak distance. This means that at small distances, strongly protected areas are only slightly smaller than weakly protected ones; with rising distance the discrepancy increases. This applies again while the intermediate field is protected over its entire length ($x_{Su} \cong a$).

The protection volume $V_{Su=0.25}$, i.e., the volume within which the aerodynamic force exerted on bodies is reduced by at least 25% to the force in the unsheltered approach flow, is shown in dimensionless manner in Figure 10a as a function of the distance with varying porosity ϕ.

As can be seen $v'_{Su=0.25}$ increases continuously with distance with the exception of the windbreak configuration $a' = 25$ and $\phi = 52\%$. In the latter case the leeward shelter effect of the first windbreak and the windward shelter effect of the second windbreak no longer overlay. Thus two separated protection volumes are generated in the intermediate field, which are comparable in shape and size with the lee- and windward protection volumes of the respective single windbreak.

Irrespective of the aforementioned exception, the intermediate field is at least protected over the overall height of the windbreaks and over its entire length.

For higher reductions of the aerodynamic wind force – i.e., for higher protection parameters S_u – the maximum volume decreases and occurs at smaller distances of the double arrangement (Figure 10b: $S_u = 0.5$, Figure 10c: $S_u = 0.75$).

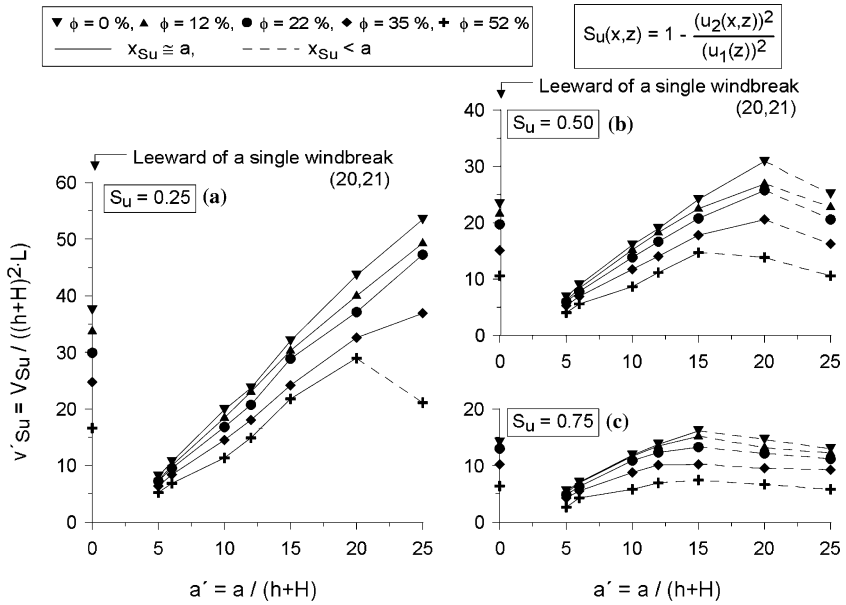

Figure 10. Dimensionless protection volume v'_{Su} as a function of distance between windbreaks a' with varying porosities ϕ for different protection parameters S_u.

At greater distances two separated protection volumes exist (Figure 7): one in the lee of the first, the other windward of the second windbreak. For very high protection parameters S_u the adequate windward protection volume can disappear.

In comparison to the leeward protection volume of single windbreaks, $V_{Su=0.25}$ can be noticeably augmented by means of a second barrier: The maximum augmentation of $\Delta V_{Su=0.25} = V_{Su=0.25}$(double-arrangement)/ $V_{Su=0.25}$(lee of single windbreak) amounts to 1.83, observed at the configuration $a' = 20$ and $\phi = 52\%$. For lower porosities the maximum occurs at higher windbreak distance ($\Delta V = 1.43(0\%) - 1.58(22\%)$ at $a' = 25$). It is expected that by a further enlargement of the distance, the size of the protection volumes still increases for these porosities, but with the used model scale the length of the wind tunnel restricts the distance which can be investigated to 25 times the windbreak height.

The maximum observed augmentation of protection volume size of an optimum double-arrangement compared to that in the lee of a single windbreak decreases with increasing protection parameter S_u

$$\begin{aligned}
&\mathrm{Max}\Delta V_{Su=0.25} = 1.83(52\%, a' = 20),\\
&\mathrm{Max}\Delta V_{Su=0.50} = 1.25(12\%, a' = 20) - 1.42(52\%, a' = 15),\\
&\mathrm{Max}\Delta V_{Su=0.75} = 1.01(35\%, a' = 15) - 1.14(0\%, a' = 15).
\end{aligned}$$

Since not every windbreak distance was investigated, of course, the maximum volume augmentations can exceed slightly the values given ahead, but it is not expected that the basic trend be changed.

The influence of porosity on the reduction of aerodynamic wind force and wind velocity in the sheltered regions can be explained physically: With increasing porosity, the kinetic energy of the approach flow in the vertical direction before the shelterbelt is weakened. As a consequence, the recirculation zone is reduced in height and length. Additionally, the amount of kinetic energy penetrating the porous belt in horizontal direction is increasing with increasing porosity, which counteracts the rotation of the recirculating mass leading to an earlier reattachment of the flow. This findings are similar to results from building aerodynamics where it is known that the distortion of the approach flow profile by a thin plate is maximum with a porosity of 0%, where we find also a maximum of recirculating mass (consistent with results shown in Section 3.4) and recirculation velocity behind the plate.

In the literature, the shelter effect of windbreaks is often assessed by the extent of protected areas. Thereby, the protected distance is the distance over which the mean velocity u_2 is reduced by a given significant percentage, such as $u_2/u_1 \leq 0.7$, where u_1 is the undisturbed upstream wind speed. The dependence of maximum extent of wind velocity reduction u_2/u_1 upon porosity is summarized in Table I for single windbreaks with and without mound. The values give the downwind distance in multiples of windbreak height at which the wind velocity recovers to 50% (in brackets 70%) of the approach velocity. From a simple transformation of Equation (13), we obtain the velocity reduction $|u_2|/u_1 = (1 - S_u)^{1/2}$ corresponding to the isolines of the protection parameter S_u. The $S_u = 0.5(0.75)$ corresponds for example to $|u_2|/u_1 \approx 0.7(0.5)$ meaning that half of the velocity causes one fourth of the aerodynamic wind force and thus a wind force reduction of 75%. For comparison, protected lengths in the lee of the upstream windbreaks of double-arrangements with a distance between the shelters of $a = 25 \cdot (h + H)$ are given in Table I.

Data derived from investigations on shelterbelts without mounds show large scatter and no uniform tendency. The classical illustration of the effect of porosity on wind shelter is that of Naegeli [5] showing that medium-dense barriers provide the greatest extent of protected area, but, unfortunately, the data sets were derived from different field studies with a variety of upstream conditions and windbreak configurations. Other measurements show an increase of protected distance with decreasing porosity for very loose to dense windbreaks, and, if any, only a slight fall-off for very dense to impermeable windbreaks, see Heisler and Dewalle [2], Wilson [29] and Table I. In contrast to recent investigations, Wang and Takle's numerical simulations [15] show that with decreasing porosity the sheltered

distance is significantly reduced near the ground and slightly reduced at higher levels. The protected lengths of our investigation agree reasonably with the data of [12, 14, 20], however, a detailed comparison is complicated by differences in upwind conditions and in surface roughness. The surface roughness determines the turbulence of the approach flow and, thus, the characteristics of the mixing layer starting at the top of the windbreak. The mixing layer spreads vertically as it moves downwind. The rate of vertical growth is determined by the turbulence of the approach flow and influences – besides the porosity – the dimensions of the sheltered regions and also the turbulence in the lee of the windbreak, see [4]. The Jensen number H/z_o describes the ratio of windbreak height H to roughness height z_o. A decrease of the Jensen number means an increase of turbulence in the approach flow and tends to lead to an decrease of protected distances, see data of [12, 14, 20] and of our investigation in Table I.

Finally, it can be summarized that the most effective double-arrangements with regard to aerodynamic wind force reduction are impermeable windbreaks. They cause the largest protection volumes. Thereby, not only the length of protected areas is increased – provided that the windbreak distance is large enough to allow this – but also their height. However, it should be noted that the turbulent kinetic energy increases simultaneously, which counteracts the mean wind reduction to a certain extent.

3.2. PEDESTRIAN COMFORT PARAMETER f BY GANDEMER

The wind protection parameter f

$$f(x, z) = \frac{u_1(z) + \sigma(u_1(z))}{|u_2(x, z)| + \sigma(u_2(x, z))} \tag{14}$$

was introduced by Gandemer [9] as pedestrian comfort parameter. This protection parameter was derived from statistical considerations and takes also the turbulent velocity fluctuations into account ($\sigma(u_i)$ =standard deviation of the mean velocity in the undisturbed ($i=1$, Pos. 1 in Figure 2) and in the disturbed flow ($i=2$, Pos. 2 in Figure 2)). If the windbreaks reduce the wind activity at a certain location, then $f > 1$, if the wind increases, then $0 < f < 1$.

In Figure 11 contour lines of three varied pedestrian comfort parameters f are given for different porosities ϕ. In Figure 12 the protection volume $v'_f = V_f/((h+H)^2 \cdot L)$ is shown exemplarily for the protection factors $f=1.5$ over the windbreak distance $a' = a/(h+H)$ for various porosities ϕ.

Assessing the shelter effect of double-arranged windbreaks with the aid of the wind comfort parameter by Gandemer, the largest influence of distance on the size of the protection volumes can be observed at low comfort parameters f. The influence of windbreak distance decreases with

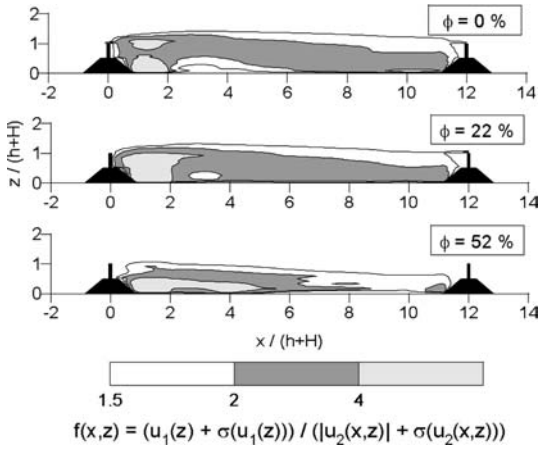

Figure 11. Contour lines of the pedestrian comfort parameter f as a function of porosity ϕ at a distance between windbreaks $a' = 12$.

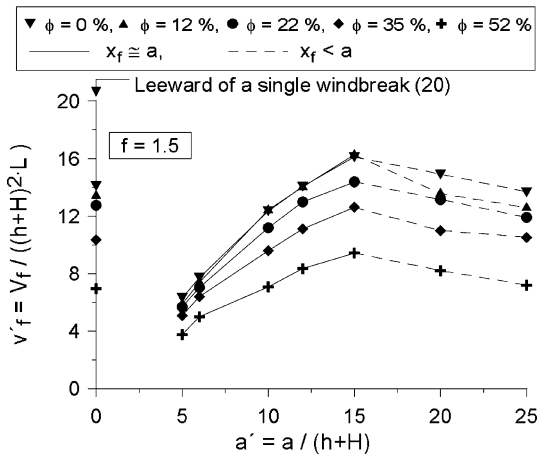

Figure 12. Dimensionless protection volume v'_f as a function of distance between windbreaks a' with varying porosities ϕ for pedestrian comfort parameter $f = 1.5$.

increasing shelter effect, since the most strongly protected areas are formed directly behind the first windward windbreak (Figure 11, $f = 4$) and are affected by the second windbreak only at very small distances.

Areas with low shelter effect ($f = 1.5$) obtain their maximum volumes at a distance of 15 times the windbreak height for all investigated porosities, whereby the size of this maximum increases with decreasing porosity. However, the difference between impermeable shelterbelts and such with a porosity of 12% is very small. At greater distances, two protected areas – one big area downstream of the windward and one small area upstream of

the leeward belt – are generated, similar as it was observed at the protection parameter S_u.

For a higher protection parameter ($f = 2$) the maximum value is no more clearly observable. Up to a distance of approximately 12 times the windbreak height for the dense and impermeable shelterbelts and of around 10 times the windbreak height for the porosity $\phi = 52\%$, the intermediate field is protected over its total length. The size of very strongly protected regions ($f = 4$) increases no longer with decreasing porosity. That is in accordance with Ruck and Lieff [13], who showed the detachment of regions with $f = 3$ in the near lee of thin artificial windbreaks without mound with increasing porosity.

Perera [10] investigated fences in a wind tunnel with porosities ranging from 0% up to 50%. He used the reciprocal value of the Gandemer parameter defined in Equation (14) and found that 10% porous fences (without mound) provides the best overall shelter, whereas impermeable fences provides the highest shelter in the immediate vicinity of the fence. From his contour plots it can be seen that the difference in size of low protected areas is small for fences with porosity ranging between 0% and 20%.

3.3. PROTECTION PARAMETER $S_{u'w'}$

The turbulence quantity $\overline{u'w'}$ describes the intensity of the turbulent vertical exchange (the turbulent vertical flux) at a certain location in the flow field. The deduced protection parameter $S_{u'w'}$ relates this exchange quantity of the disturbed flow field (Pos. 2 in Figure 2) to the same quantity of the undisturbed approach flow (Pos. 1 in Figure 2):

$$S_{u'w'}(x, z) = 1 - \frac{\overline{u'w'}_2(x, z)}{\overline{u'w'}_1(z)}. \tag{15}$$

Because the mean horizontal velocity of the approach flow increases with height, $\overline{u'w'}_1(z)$ of the undisturbed flow is negative by convention [26, 30]. This means that turbulent eddies transport momentum downwards. Thus, this protection parameter is useful to assess the efficiency of windbreak systems with respect to the vertical turbulent transport

$0 < S_{u'w'} < 2$: reduced momentum exchange in vertical direction,

$S_{u'w'} < 0$: increased momentum exchange to the ground,

$S_{u'w'} > 2$: increased momentum exchange away from the ground.

Figure 13 shows contour lines of the protection parameter $S_{u'w'}$ for various porosities. Protection volumes with reduced momentum exchange in vertical direction ($0 < S_{u'w'} < 2$) are indicated as grey areas without contours. They run near the ground and extent up to windbreak height in the near

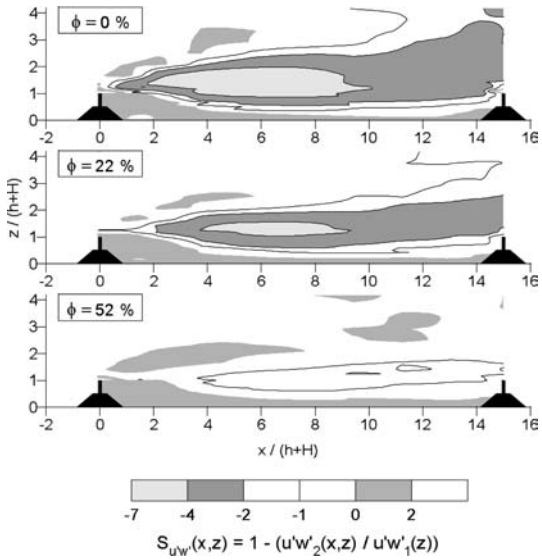

Figure 13. Contour lines of the protection parameter $S_{u'w'}$ as a function of porosity ϕ at a distance between windbreaks $a' = 15$.

lee of the upstream windbreaks. Further downstream their vertical extensions are rather small.

Above these protection volumes 'wake' zones are formed with covariances greater than those in the approach flow and with increased momentum exchange to the ground ($S_{u'w'} < 0$). In Figure 14 the protection

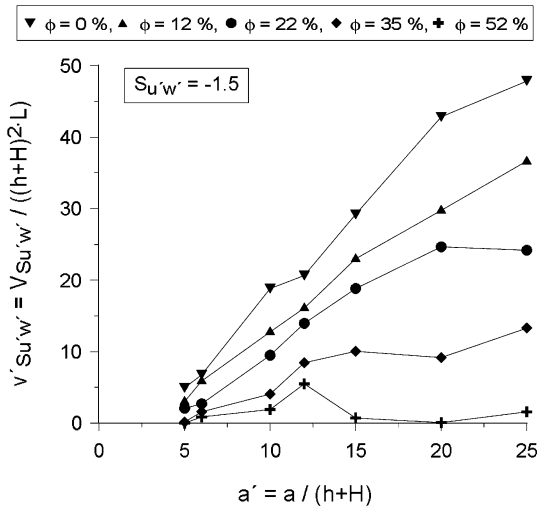

Figure 14. Dimensionless protection volume $v'_{Su'w'}$ as a function of distance between windbreaks a' with varying porosities ϕ for protection parameter $S_{u'w'} = -1.5$.

volume $V_{Su'w'}$ is shown over the windbreak distance $a' = a/(h + H)$ for different porosities ϕ and for the parameter $S_{u'w'} = -1.5$. That means that the momentum exchange is at least 2.5 times as much as in the undisturbed flow. As can be seen, the area with $S_{u'w'} = -1.5$ increases with decreasing porosity.

Furthermore it was observed that with decreasing porosity the momentum exchange to the ground increases. The extreme value of this protection parameter (averaged over the investigated distances) amounts to $S_{u'w'} = -1.94$ for medium dense windbreaks ($\phi = 52\%$) and $S_{u'w'} = -5.64$ for impermeable windbreaks. The increase of the turbulent momentum flux with decreasing porosity in the mixing layer can be explained by the increasing velocity gradient of the distorted wind profiles.

The investigations about single line shelterbelts with mound show the same tendencies, but the magnitude of increase of momentum exchange differs [20]. The $S_{u'w'}$-values are higher, but this can rather be attributed to the lower $u'w'$-values of the undisturbed flow than to enhanced values in the disturbed flow.

For single shelterbelts without mound, Wang and Takle [31] noted that at $z = H/2$ the turbulent flux $u'w'_2$, normalized by the upstream undisturbed turbulent flux at the height of the shelterbelt $u'w'_{1H}$, is reduced in the near lee and enhanced in the middle lee, whereas at $z = 2H$ the turbulent flux is enhanced throughout. Thereby the magnitude of the enhanced wake turbulence increases likewise with decreasing porosity and the maximum moves toward the shelterbelt.

3.4. RECIRCULATION ZONES

For small porosities, a separation of the flow occurs at the windbreak forming a region with rotating fluid mass on the leeward side. Such recirculation zones can be visualized by displaying the measured data in streamline plots. Depending on the porosity, recirculation zones can or cannot occur, in any case, however, the wind-protected area is much greater than any possible recirculation zone.

Figure 15 shows streamlines $\psi \leq 0$ for different porosities. In Figure 16 the recirculation volumes and the reattachment lengths are laid on in dimensionless form over the windbreak distance for different porosities.

As long as the distance of the windbreaks is smaller or equal than the reattachment length x_{Rez} (the distance in which the separation streamline hits the ground), the separated air mass rotates over the entire intermediate area. Then the leeward windbreak affects the size of the recirculation volume. As soon as the distance of the double-arranged windbreaks is slightly bigger than the reattachment length, a small increase of the reattachment length can occur (this was observed at 10-fold windbreak distance for the

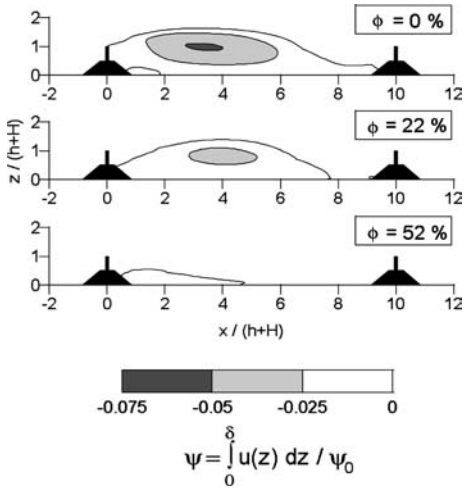

Figure 15. Recirculation zones as a function of porosity ϕ at distance between windbreaks $a' = 10$.

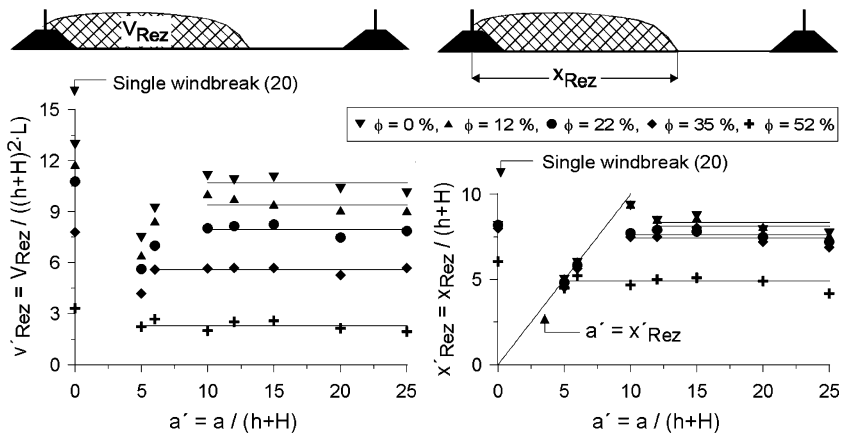

Figure 16. Dimensionless recirculation volume v'_{Rez} and reattachment length x'_{Rez} as a function of porosity ϕ and distance between windbreaks a'.

porosities 0% and 12%) which disappears however with a further enlargement of the distance. However, the extended recirculation zone shows only a small height. Thus, it contributes only insignificantly to an enlargement of the recirculation volume size.

At greater windbreak distances, the reattachment lengths and the sizes of recirculation volumes remain nearly constant and agree well with those of the single windbreak from the investigations of Ruck and Donat [20].

Furthermore, the recirculation volume increases with decreasing porosity. This applies for all investigated distances and agrees with the behaviour of the single windbreak [20]. The extent of the recirculation areas in

mainstream direction increases – as soon as the distance of the windbreaks permits it – with decreasing porosity. Thereby, the difference in reattachment length is much larger between porosities of $\phi = 52\%$ and $\phi = 35\%$ than between porosities of $\phi = 35\%$ and $\phi = 0\%$.

Perera [10] noted that recirculation zones in the lee of porous fences decrease in size as the fence porosity increases and move downstream. Furthermore, he observed that recirculating bubbles exist only for porosities less than 30%. Ruck and Lieff [13] still observed a recirculation zone behind 30% porous shelterbelts without mound but no more behind 50% porous ones. This is in accordance with Wang and Takle [15]. Both found out that as the porosity increases the seperation point moves downstream and the bubble height decreases.

3.5. KINETIC ENERGY

As mentioned before, the protection parameter S_u does not account for the gustiness of wind. Since the decrease of mean wind velocity in the wind-reduced areas is usually associated with an increase in turbulent kinetic energy, this quantity is also of interest.

In Figure 17 contour lines of the relative turbulent kinetic energy $\mathrm{TKE_{rel}}$ are displayed for different porosities. At this, $\mathrm{TKE_{rel}}$ is the increase of the local turbulent kinetic energy TKE in the intermediate field of the windbreaks (Pos. 2 in Figure 2) referred to the TKE in the undisturbed approach flow (Pos. 1 in Figure 2) at the same height:

$$\mathrm{TKE_{rel}}(x, z) = \frac{\mathrm{TKE_2}(x, z)}{\mathrm{TKE_1}(z)}, \tag{16}$$

$$\mathrm{TKE}(x, z) = 0.75 \cdot (u'(x, z)^2 + w'(x, z)^2). \tag{17}$$

Obviously, the shape of areas of increased $\mathrm{TKE_{rel}}$ is similar to those of increased vertical momentum exchange (Figure 13). $\mathrm{TKE_{rel}}$ decreases generally with increasing porosity. This is consistent with the findings of [15,20]. This decrease of $\mathrm{TKE_{rel}}$ can be attributed again to the fact that the intensity of the shear layers (the distortion of the velocity profiles) decreases with increasing porosity. For impermeable windbreaks, the mean value of $\mathrm{TKE_{rel}}$ over all distances amounts to 4.84 and the maximum value is 5.53 at a distance $a' = 20$. For the porosity $\phi = 52\%$, the distance-averaged value of $\mathrm{TKE_{rel}}$ amounts to 2.25 and the maximum value is 2.68 measured at a distance $a' = 12$.

Regarding the configuration with maximum increase of the turbulent kinetic energy, $\mathrm{TKE_{max}}$ is still small compared to the overall kinetic energy of the undisturbed flow $\mathrm{GKE_1}$ ($\mathrm{TKE_{max}}$ / $\mathrm{GKE_1}$ = 0.37). Thereby the GKE

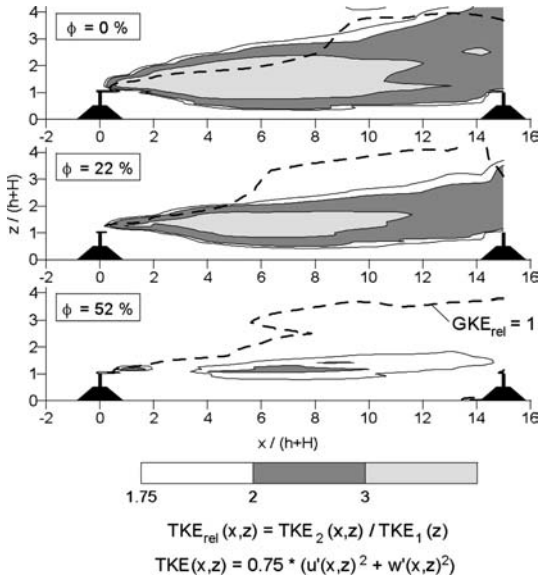

Figure 17. Contour lines of the relative turbulent kinetic energy TKE_{rel} as a function of porosity ϕ at distance between windbreaks $a' = 15$. The dashed line plots the relative overall kinetic energy $GKE_{rel} = 1$. For regions under this line apply $GKE_{rel} < 1$, for regions above $GKE_{rel} > 1$.

is the sum of the mean kinetic energy MKE and the TKE

$$GKE = MKE + TKE \tag{18}$$

with

$$MKE(x, z) = 0.5 \cdot (u(x, z)^2 + w(x, z)^2) \tag{19}$$

and TKE as defined in Equation (17).

The relative overall kinetic energy GKE_{rel} (the ratio of the overall kinetic energy in the intermediate field referred to the overall kinetic energy of the approach flow) decreases in the area under the dashed line shown in Figure 17 and thus in the lower part of the intermediate field at least up to windbreak height.

4. Conclusions

The systematic wind tunnel study about the influence of shelterbelt porosity and windbreak distance on the wind reduction in the intermediate field of double-arranged mound-mounted shelterbelts shows:

– The optimum windbreak distance depends on the desired shelter efficiency (i.e., the protection parameters S_u and f) and on the porosity. Decreasing these quantities, the optimum windbreak distance increases.

– The double-arrangement is effective particularly for low to medium protection parameters S_u. If high shelter effects are required a second windbreak contributes scarcely anything to an augmentation of the protection volume.
– The size of the protection volumes increases with decreasing porosity, with decreasing protection parameter S_u and with increasing windbreak distance, respectively. This applies so long as the intermediate field is protected over its whole length. When the windbreak distance is larger, protection volumes leeward of the first and windward of the second windbreak are generated, comparable to those lee- and windward of a single windbreak. In this case, the size of the protection volumes remains constant by a further enlargement of windbreak distance.
– The vertical momentum exchange and the relative turbulent kinetic energy increases with decreasing porosities in the "wake" of the first windbreak. On the other hand, the relative overall kinetic energy decreases at the same time at least up to windbreak height.

Acknowledgement

The authors would like to thank the Deutsche Bundesstiftung Umwelt (DBU) in Osnabrück for the financial support of this investigation within the project No. 18062.

References

1. Van Eimern, J., Karschon, R., Razumova, L.A. and Robertson, G.W.: 1964, *Windbreaks and Shelterbelts,* Technical Note No. 59, World Meteorological Organization, 188 pp.
2. Heisler, G.M. and DeWalle, D.R.: 1988, Effects of windbreak structure on wind flow, *Agric. Ecosyst. Environ.* **22/23**, 41–69.
3. McNaughton, K.G.: 1988, Effects of windbreaks on turbulent transport and microclimate, *Agric. Ecosyst. Environ.* **22/23**, 17–39.
4. Cleugh, H.A.: 1998, Effects of windbreaks on airflow, microclimates and crop yields, *Agroforestry Syst*. **41**, 55–84.
5. Nägeli, W.: 1945, Weitere Untersuchungen über die Windverhältnisse im Bereich von Windschutzstreifen, *Mitteil. Schweizer. Anstalt für das forstl. Versuchswesen* **24**, 659–737.
6. Sturrock, J.W.: 1969, Aerodynamic studies of shelterbelts in New Zealand – 1, low to medium height shelterbelts in Mid-Canterbury, *N.Z J. Sci.* **12**, 754–776.
7. Sturrock, J.W.: 1972, Aerodynamic studies of shelterbelts in New Zealand – 2, medium-height to tall shelterbelts in Mid-Canterbury, *N.Z J. Sci.* **15**, 113–140.
8. Nord, M.: 1991, Shelter effects of vegetation belts – Results of field measurements, *Boundary-Layer Meteorol.* **54**, 363–385.
9. Gandemer, J.: 1981, The aerodynamic characteristics of windbreaks, resulting in empirical design rules, *J. Wind Eng. Ind. Aerodyn*. **7**, 15–36.

10. Perera, M.D.A.E.S.: 1981, Shelter behind two-dimensional solid and porous fences, *J. Wind Eng. Ind. Aerodyn*. **8**, 93–104.
11. Klingbeil, K., Benndorf, D. and Grunert, F.: 1982, Aerodynamische Grundlagen für Windschutzpflanzungen – Der Einfluß der Geometrischen Struktur von Gehölzschutzstreifen auf ihre Schutzwirkung, Teil II, *Z. Meteorol.* **32**, 165–175.
12. Raine, J.K. and Stevenson, D.C.: 1977, Wind protection by model fences in a simulated atmospheric boundary layer, *J. Ind. Aerodyn.* **2**, 159–180.
13. Ruck, B. and Lieff, W.: 1997, Wind tunnel simulation of shelter belt performance. In: B. Ruck, A. Leder and D. Dopheide (eds.), *Laser Anemometry – Advances and Applications*, University of Karlsruhe, pp. 577–586.
14. Lieff, W.: 1993, *Vergleich der Umströmung von Bäumen in Natur und Modell*, Diploma thesis, ifH, University of Karlsruhe.
15. Wang, H. and Takle, E.S.: 1995, A numerical simulation of boundary-layer flows near shelterbelts, *Boundary-Layer Meteorol.* **75**, 141–173.
16. Wang, H., Takle, E.S. and Shen, J.: 2001, Shelterbelts and windbreaks: mathematical modeling and computer simulations of turbulent flows, *Annu. Rev. Fluid Mech.* **33**, 549–586.
17. Judd, M.J., Raupach, M.R. and Finnigan, J.J.: 1996, A wind tunnel study of turbulent flow around single and multiple windbreaks, Part 1: Velocity fields, *Boundary-Layer Meteorol.* **80**, 127–165.
18. McAneney, K.J., and Judd, M.J.: 1990, Multiple windbreaks: an aeolean ensemble, *Boundary-Layer Meteorol.* **54**, 129–146.
19. Wilson, J.D. and Yee, E.: 2003, Calculation of winds disturbed by an array of fences, *Agric. For. Met.* **115**, 31–50.
20. Ruck, B. and Donat, J.: 2000, *Einfluss der Geometrie von Sockelwällen auf die Wirksamkeit von Windschutzpflanzungen*, Final Report of DBU research project 12071.
21. Ruck, B.: 2001, Efficiency of shelterbelts on mounds, *Proceeding of PHYSMOD2001*, University of Hamburg.
22. Counihan, J.: 1975, Adiabatic atmospheric boundary layers: A review and analysis of data from the period 1880–1972, *Atmos. Environ.* **9**, 871–905. (Pergamon Press)
23. WTG-Merkblatt, Windkanalversuche in der gebäudeaerodynamik: 1995, In: E.J. Plate, (ed.), *Windprobleme in dichtbesiedelten Gebieten*, WTG-Berichte Nr. **3**, pp. 241–284, Windtechnologische Gesellschaft, Aachen.
24. Eurocode 1: Basis of design and actions on structures, part 2.4: Wind actions, ENV 1991–2–4. In: H.-J. Niemann (ed.), 1994, *Windlastnormen nach 1992*, WTG-Berichte Nr. **2**, pp. 165–286, Windtechnologische Gesellschaft, Aachen.
25. Rotta, J.C.: 1972, *Turbulente Strömungen*, B.G. Teubner, Stuttgart.
26. Stull, R.B.: 1988, *An Introduction to Boundary-Layer Meteorology*, Kluwer Academic Publishers, Dordrecht.
27. Plate, E.J.: 1995, Windprofile in der Gebäudeaerodynamik. In: E.J. Plate, (ed.) *Windprobleme in dichtbesiedelten Gebieten*, WTG-Berichte Nr. 3, pp. 7–26, Windtechnologische Gesellschaft, Aachen.
28. Wilson, J.D.: 1987, On the choice of a windbreak porosity profile, *Boundary-Layer Meteorol.* **38**, 37–49.
29. Wilson, J.D.: 1985, Numerical studies of flow through a windbreak, *J. Wind Eng. Ind. Aerodyn*. **21**, 119–154.
30. Garratt, J.R.: 1994, *The Atmospheric Boundary Layer*, Cambridge University Press, Cambridge.
31. Wang, H. and Takle, E.S.: 1996, Momentum budget and shelter mechanism of boundary-layer flow near a shelterbelt, *Boundary-Layer Meteorol.* **82**, 417–435.